SURFACE PHOTOVOLTAGE STUDIES OF OPTOELECTRONIC PROCESSES OBSERVED IN SOME POLYMER-BASED THIN FILMS

by

Christopher Harms

Submitted in partial fulfillment of the
requirements for Departmental Honors in
the Department of Physics & Astronomy
Texas Christian University
Fort Worth, Texas

May 2, 2016

SURFACE PHOTOVOLTAGE STUDIES OF OPTOELECTRONIC PROCESSES OBSERVED IN SOME POLYMER-BASED THIN FILMS

Project Approved:

Supervising Professor: Yuri Strzhemechny

Department of Physics & Astronomy

Anton Naumov

Department of Physics and Astronomy

Tristan Tayag

Department of Engineering

ABSTRACT

The lower production costs of organic photovoltaic (OPV) solar cells vs. traditional inorganic architectures could provide a more cost-effective alternative for the solar power industry. We studied layered OPV samples of P3HT:PCBM/ZnO/ITO/glass employing surface photovoltage (SPV) measurements. The SPV experiments were performed via the Kelvin probe approach in a vacuum chamber filled with a 100% nitrogen gas at atmospheric pressure. The data was collected both as a function of time for a polychromatic illumination and as a function of photon energy for a monochromatic illumination. ZnO/ITO/glass and ITO/glass structures were also probed as control samples. The P3HT:PCBM/ZnO/ITO/glass specimens were synthesized with variations of growth/deposition/processing temperatures of both P3HT:PCBM and ZnO. The addition and variations of synthesis conditions of the active layer produced significant changes in the observed "light-on" and "light-off" SPV transients, which revealed fast and slow charge recombination processes (in contrast with, e.g., the ZnO/ITO/glass samples yielding only one "standard" recombination time). Presence of the active layer and its growth conditions also dramatically affected the SPV spectroscopy data. Furthermore, both the transient and spectral SPV results were dependent on the growth/deposition conditions of the ZnO layers. The multiple processes on different timescales indicate the presence of several pathways for surface/interface charge recombination. Whether the long-term recession of the voltage-against-time values is a factor of the specimens or due to atmospheric adsorption or some other cause is yet to be determined and requires further study.

Polysulfone, a high-strength thermoplastic, possesses a variety of applications such as dielectric material, membranes, filters, space travel, and microfluidics. First, we developed a reliable method to create thin polysulfone films of varying thicknesses through spin coating on n-doped silicon substrates. After enough suitable samples were prepared with thin films of various thicknesses, the samples were subjected to surface photovoltage testing. The introduction of the polysulfone layer caused a red-shifting of the silicon band gap as well as creating more features in the near-infrared spectral region. The polysulfone also caused a reverse in the polarity of the short-term transient process of the surface under illumination. Under the influence of ultraviolet light, polysulfone reverses its normal hydrophobic nature to a hydrophilic state for a limited time. Measurement of such a surface revealed more short-term transient features under illumination as well as the accentuation of the near-infrared features attributable to polysulfone. Whether the transient features unique to the UV-exposed surface are inherent properties of the hydrophilic surface or artifacts of the reversion process is a matter for future testing.

Introduction

Water striders resting on the surface of a pond provide an everyday reminder that properties and effects at the surface of a material are not necessarily the same as those of the bulk material. We might hope to find the next scientific "miracle" (or at least some interesting and useful properties) at the surface level through our investigations into thin layers of polymers.

Experiments were carried out on two separate projects. First, a set of organic photovoltaic devices (OPVs) were analyzed, seeking information on the effects of various layers on the surface and buried interface states. Bulk Heterojunction (BHJ) solar cells, a subgroup of OPVs, are a type of thin film solar cell that uses polymer chains coupled with another material, in this case a fullerene, to split electrons and produce electricity via the photovoltaic effect. A photon strikes the polymer which ejects an electron, which then transfers over to the fullerene phase, traveling to a conducting layer and creating electricity. These two materials can be combined such that instead of a flat surface, a deposited solution will dry with the phases separating somewhat, forming a large contact area for charge dissociation.

While doped silicon solar cells require vacuum in their production, these polymer solar cells can be spin coated, providing a significant decrease in manufacturing costs. Furthermore, these BHJ solar cells can be placed on a flexible substrate, and they may also demonstrate some amount of transparency, both of which open up a wide variety of potential new applications, such as the windows of office buildings. Unfortunately, these new solar cells are not nearly as efficient as their crystalline silicon counterparts, which largely negates the advantage in production costs, as well as undergoing photodegredation, which significantly limits their lifespan. There currently exists a rough parity in cost per kilowatt

hour between traditional silicon solar cells and BHJ cells, this "quality versus quantity" tradeoff could be upset by future findings in the field.[1,2]

The second project focused on polysulfone, a material for which the surface states are not well-known. Made up of long chains of sulfone monomers, polysulfone is a thermoplastic with high hydrolysis stability, which gives it advantageous characteristics for use in water filtration devices. While thin films of polysulfone are naturally hydrophobic, exposure to ultraviolet (UV) light causes these surfaces to become hydrophilic. If one side of a thin polysulfone mesh is treated with UV radiation and water is placed on this side, the mesh would then exhibit a diode-like behavior, allowing water to flow primarily in one direction. If the pores of the mesh were made small enough, they could be used for a wide variety of filtration and microfluidics applications.[3]

Due to the thin nature of the examined layers of both experiments, we wish to investigate their surface and interface optoelectronic properties to provide significant contributions to the overall electronic properties of the material. We shall use Surface Photovoltage to probe these characteristics.

Surface Photovoltage

At the surface of a material, various physical and chemical deviations, such as dangling bonds and chemical changes, can create trap states. Electrons emitted due to the photovoltaic effect when the sample is illuminated may proceed to get caught in these traps, creating a variation in charge distribution, which results in an electric field and a potential drop across this field as seen in Figure 1. To test this, a piece of metal would be placed close (but not in

1 D. Szostak, B. Goldstein, Appl. Phys. Lett. 56, 522 (1984).
2 B. Goldstein, D. Redfield, D. Szostak, L. Carr, Appl. Phys. Lett. 39, 258 (1981).
3 E. Bormashenko, S. Balter, A. Makin, D. Aurbach, *Maromol. Mater. Eng.* 2014, 299:27-30.

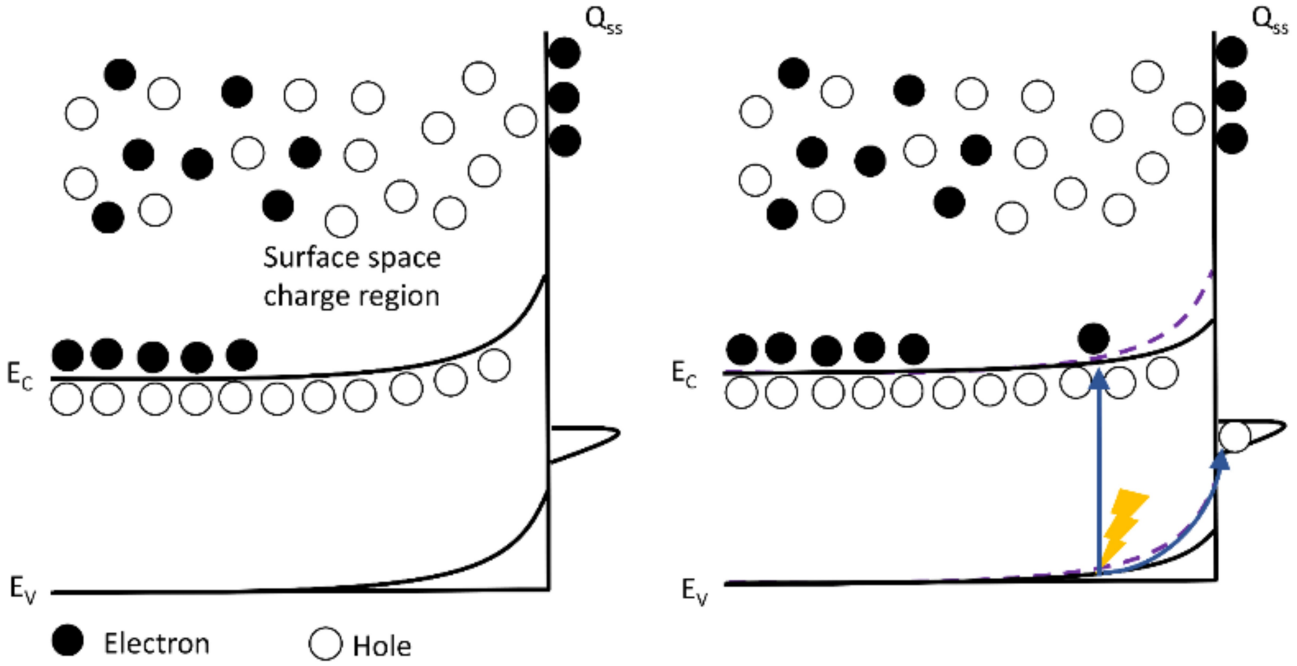

Figure 1: Surface photovoltage diagram showing the transition of an electron to a trap state, creating a change in the circuit voltage.

contact with) the surface, forming a parallel plate capacitor. The potential drop across the capacitor is known as the contact potential difference (CPD) of the system. The CPD may be found by measuring what bias voltage is sufficient to discharge the capacitor. This testing format is known as a Kelvin probe. The Kelvin probe used here has a vibrating plate held above the surface while computer systems are used to vary the vibrations such that they create a steady-state alternating current in the capacitor. The capacitor is discharged when this AC current is 0. Therefore, the CPD is equal to the bias voltage of the circuit for which the AC current is 0.[4]`

For the BHJ solar cells, we utilize surface photovoltage to investigate the deviations caused by the addition of each layer to the structure, as well as the effects of different annealing temperatures for each layer. The surface photovoltage of polysulfone films was first examined as a function of thickness. Next, knowing that the hydrophobicity of the material

4 L. Kronik, Y. Shapira, *Surf. Interface Anal*. 2001; 21:954-965

changes when exposed to ultraviolet light, a sample was exposed to UV light and then its surface photovoltage measurements were compared to those of the unaltered sample.

Surface Photovoltage Studies of Bulk Heterojunction Solar Cells

Solar Cell Synthesis

All the solar cell samples were prepared in the Laboratory of Printed Electronics and Solar Cells of Wroclaw Research Centre EIT+ in Wroclaw, Poland. Each of the samples begins as a piece of Polish glass. First, Indium Tin Oxide (ITO), the electron transport layer, is deposited on the substrate to a thickness of 100 nm. Next, an approximately 40 nm thin film of Zinc Oxide (ZnO) is deposited on top of the ITO layer. The Glass/ITO/ZnO samples are then divided and annealed at two different temperatures, 300°C and 500°C. Two of each of the annealed samples are spun with a bulk heterojunction layer of P3HT:PCBM about 200 nm thick. These pairs are then split up, with one annealed at a lower temperature of 110°C, while the other is annealed at 170°C.

This synthesis process yielded the seven samples that were tested. These are:

TCU0: Glass/ITO

TCU1: Glass/ITO/ZnO (300°C)

TCU2: Glass/ITO/ZnO (300°C)/P3HT:PCBM (110°C)

TCU3: Glass/ITO/ZnO (300°C)/P3HT:PCBM (170°C)

TCU4: Glass/ITO/ZnO (500°C)

TCU5: Glass/ITO/ZnO (500°C)/P3HT:PCBM (110°C)

TCU6: Glass/ITO/ZnO (500°C)/P3HT:PCBM (170°C)

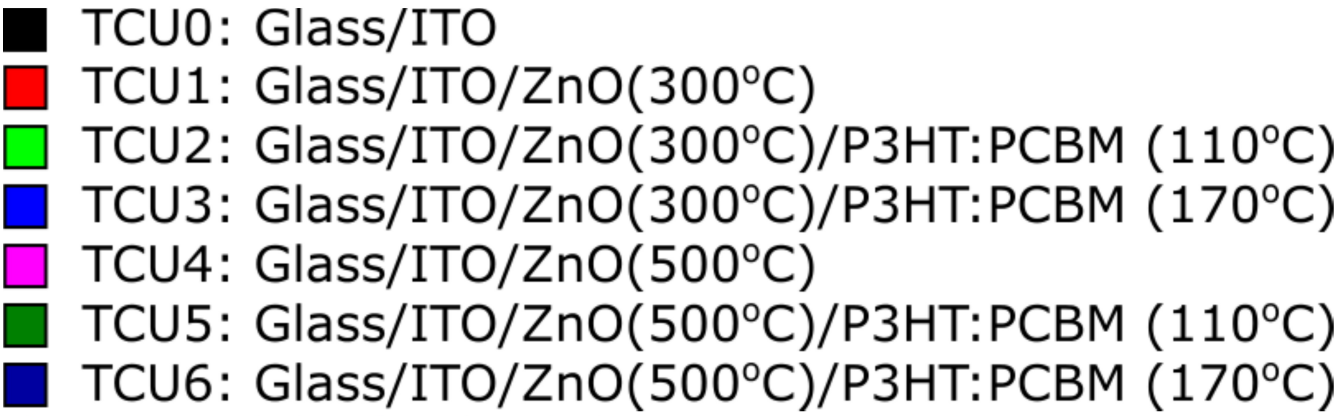

Figure 2: Listing of solar cell samples and color key for comparison graphs.

Experimental

To test the solar cell samples, an (almost) closed circuit needs to be completed through the BHJ layer. The specimens are mounted on conductive metal sleds with conductive carbon tape. Unfortunately, this is not enough, as the vast majority of the vertical cross-section of the samples is composed of glass, a strong insulator. Therefore, a connection between the ITO (electron transport) layer and the stage is needed. This is accomplished by using a small piece of indium, held in place by a carbon tape covering, to connect the two. The choice of indium was made for two properties: the first is its high malleability and low hardness, allowing us to mold it into the desired shapes, and the low contact potentials created at the contact points.

After the sample is secured in place on the stage, the stage is loaded into the vacuum chamber, filled with pure nitrogen gas at atmospheric pressure. From the load/lock chamber, the stage is transported to the testing chamber via a telescoping arm. Once there, the stage is placed in the basket of an XYZ manipulator, which will then raise the stage into the testing position. To complete the circuit, the stage must be in contact with a conducting copper wire while simultaneously having the surface of interest on the sample directly underneath the Kelvin probe, with the two separated by less than 1 mm. Before each test, the sample was

allowed to desaturate in the darkened chamber, allowing any electrons in the surface states to relax back to their normal bulk states. The sample is then ready for its time in the light.

To illuminate the sample, light passes through a fiber optic cable, entering in the vacuum chamber next to the Kelvin probe and above the surface of interest. The type of testing determines which light source is attached to the other end of the fiber. For transient voltage testing, the fiber connects to a Fiber-Lite 190 white light source, which is set to medium intensity. Using Labview, the voltage of the circuit through the sample and the Kelvin probe is tracked, measuring the effect that sustained exposure to white light has on the voltage. Transient tests are limited by the maximum storage of the Labview program. After ascertaining that the surface states have reached an equilibrium saturation level (as evidenced by an unvarying voltage on a logarithmic time scale), the light source is doused and the voltage is monitored as the electrons relax to their equilibrium states.

When the spectroscopic data was desired, the fiber was attached to a monochromator assembly. In this assembly, radiation from a Ushio 24 V 250 W xenon bulb is passed through a Newport 1/8 m monochromator and the light is passed through a bandpass filter to remove higher-order diffraction effects. To acquire the requisite f-number for total internal reflection, the single wavelength is passed through an f-number matcher (also from Newport), and is then sent into the fiber optic cable. The lower limit in terms of wavelength is set by fiber optic cable; the glass becomes opaque to wavelengths shorter than about 300 nm.

Solar Cell Data and Analysis

Light On SPV Transients

The data collected of the transient voltage under illumination provides a glimpse into the electronic movement in the samples based upon the varying layers. The TCU0 sample

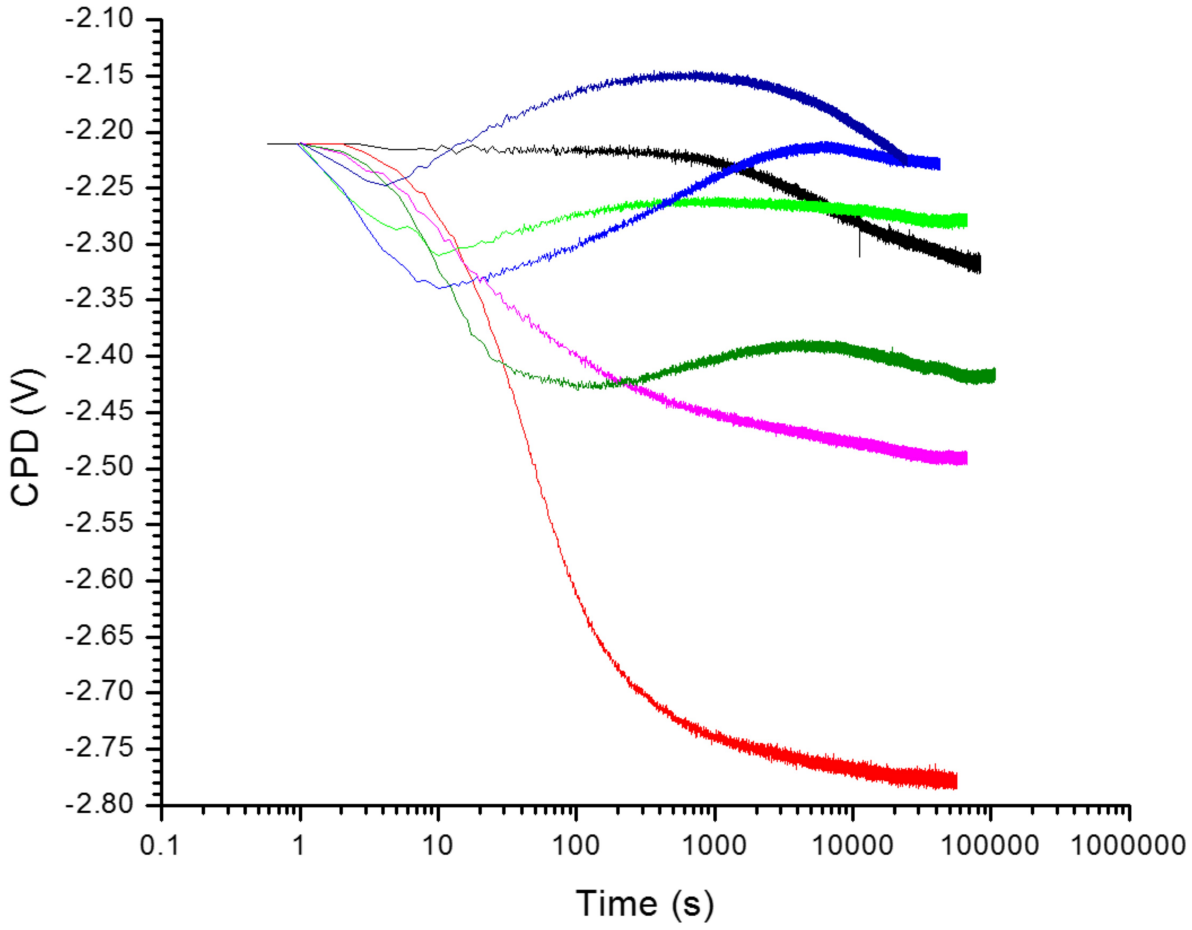

Figure 3: Comparison of representative transient data from illuminated solar cell samples.

shows a transient voltage change that is relatively modest in magnitude and takes a very long time to occur. (no There is noticeable voltage deviation until ~10^4 s under illumination, and the total change was on the order of 0.1 V. Therefore, the contributions from the Polish glass and ITO layers are appreciable, but realistically, they are small compared to those of later sample layers on a typical day/night time scale (~$5x10^4$ s).[5]

Next, TCU1 and TCU4 demonstrate the contributions of the ZnO layer at the two different annealing temperatures. TCU1 (annealed at 300°C) possesses the largest voltage differential of all the samples, about 0.6 V, and occurs almost immediately upon illumination,

5 O. Mryasov, A. Freeman, Phys. Rev. B 64: 233111 (2001).

tapering off in the 10^4-10^5 s range. This large change in voltage corresponds to a large charge accumulation in the surface trap states. When plotted with time on a log scale, the data forms a logistic curve with an inflection point at ~40 s. The data from TCU4 (annealed at 500°C) bears some similarities to that of TCU1, but there are also some differences. The most noticeable difference is the magnitude of the change in voltage, about half the magnitude of TCU1's change. The logistic curve shape is still present, but the inflection point in the graph of the data occurs at ~20 s, twice as soon as that of TCU1. This suggests that the annealing temperature does have some effect on the SPV properties of the samples. Zinc oxide actually possesses a higher decomposition point (1975°C) than ITO does (1526-1926°C), so the annealing may have an effect on both layers. Unfortunately, the contributions cannot be separated without testing of specimens with only a ZnO layer. Due to SPV measurements generally recording the largest signals from the uppermost surface, it is likely that the change in response is due to the changes in the ZnO layer, possibly an increase in ZnO crystal size from annealing.

Finally, the contribution from the BHJ layer must be considered. All four of the samples that include a BHJ layer appear to have multiple processes going on, as evidenced by the complex curves of the data that appear to start as a logistic curve and then transition to a sinusoidal curve. This is likely indicative of surface states quickly becoming saturated in the short term, then finding one or more paths for electrons to either reenter the bulk of the layers or transitioning to states present at the buried interfaces. As one might expect with two values for each of the two annealing temperatures, the samples can be paired up based on similarities (sharing relative maxima and minima at approximately the same time) in the graphs of their data. One of these pairs contains TCU2 and TCU6, the other includes TCU3 and TCU5. Interestingly, the members of each share neither the ZnO annealing temperature

nor the BHJ annealing temperature, which could indicate that another undeclared variable might be influencing the electronic processes.

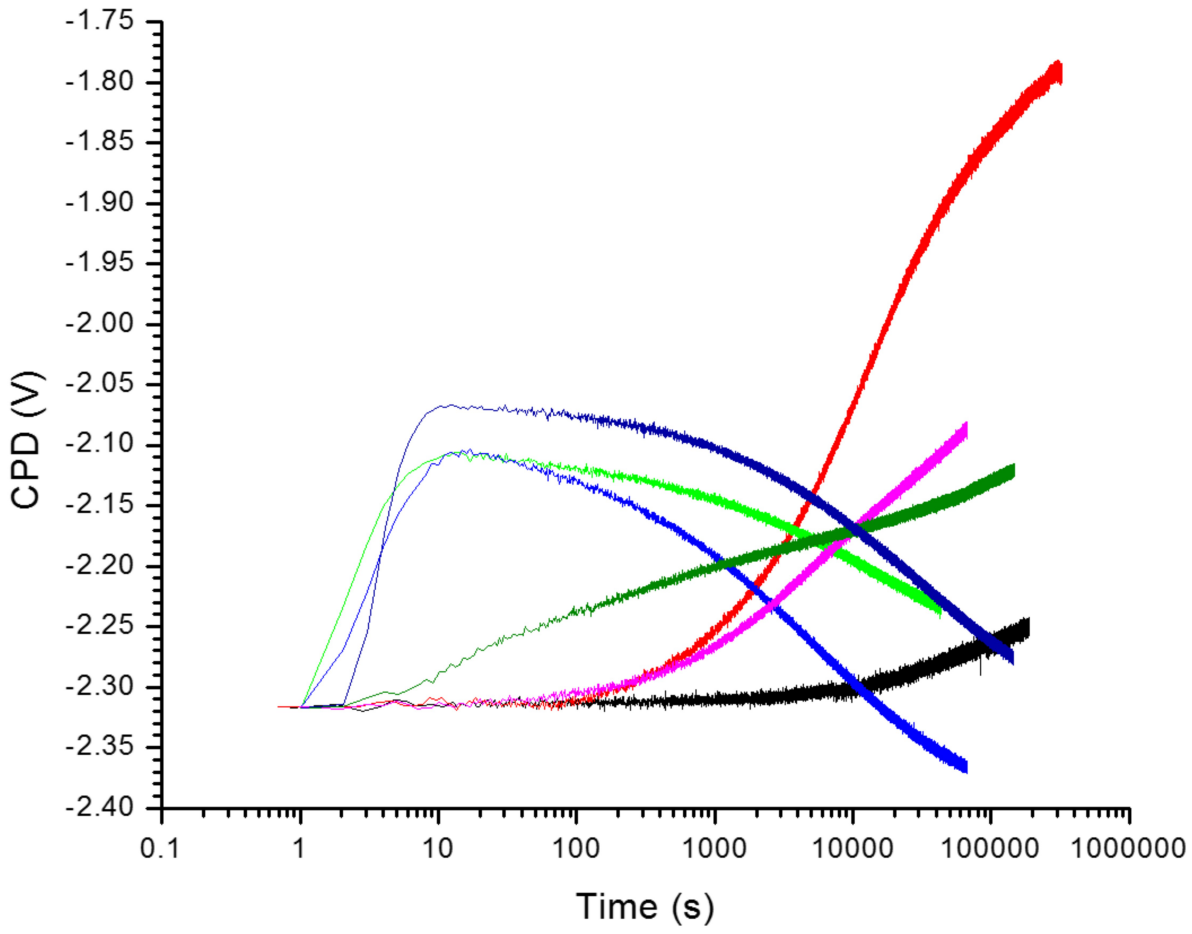

Figure 4: Comparison of representative transient data from solar cell samples in the dark after illumination.

Light Off SPV Transients

The data of the voltage of the darkened samples may also be divided up based on the layers present on each specimen. The graph of TCUo, which consists of only ITO and the glass substrate, has only a small change in voltage from a very long-lived process, only

becoming noticeable after ~10^5 s in darkness. As the average period of night on Earth is about $4.3x10^4$ s, this process would produce little variation in potential ground-mounted systems in tropical and temperate latitudes.

The graph of TCU1 shows the largest positive change in voltage, which corresponds nicely to the large negative change when illuminated; the large quantity of electrons that accumulated in the surface states created about 0.6 V change, and their relaxation would have likely resulted in a return to the same initial voltage given enough time. The relaxation data, like the illumination data, fits a logistic curve with an inflection point around $1x10^4$ s. This TCU4 sample data, like its illumination counterpart, bears many of the same characteristics as the TCU1 relaxation data, just with a smaller change in voltage.

After being left illuminated for more than two days each, the samples with the BHJ layer were assumed to have reached equilibrium electron saturation, allowing the relaxation effects to be tested. Samples TCU2, TCU3, and TCU6 all possess a similar general shape in the time domain measured, consisting of a fast process on the order of 10^0-10^1 s that causes an increase in voltage, coupled with a much slower decreasing process with an inflection point on the order of 10^4-10^5 s. This likely represents the electrons in the surface states quickly relaxing back into the bulk, but the contrary slow process could have a number of interpretations. TCU5 is the odd sample out in this group; its graph shows at least two evident processes, both of which are positive. The faster change likely is a contribution from the electrons trapped in surface states returning to their bulk states, while the slower process may be due to electron transport and capture at buried interfaces.

SPV Spectroscopy

The graphs of the spectroscopic data collected from each sample may be found in

Appendix A. Six spectroscopic runs were performed on TCU0, three with each filter set. While the individual data sets appear random compared to those of other samples, the voltage scale is much lower, so the ITO and glass do not appear to react to any particular wavelengths of light in the short timescale. This is hardly surprising, as glass is an insulator with poor electron mobility and the ITO band gap can exceed 4 eV, requiring more energy than the photons delivered to the sample.[67]

Next, the graphs for TCU1 began to show much larger characteristics with the addition of the ZnO layer. The half of the graphs utilizing the second set of filters produced a feature at ~1.8 eV, while all the graphs show a significant change in voltage at 3.4 eV. This higher energy trait is due to the well-documented 3.4 eV band gap of ZnO. The lower deviation may be a second-order effect from the band gap, or it could be an artifact due to the filters affecting the intensity of the light that is passed through to the f-number matcher. If it were a second-order effect of the band gap, it should appear in all sets of data Because it only appears in the data from the one filter set near the edge of those filters' usable wavelengths, we can relatively safely assume that this element is a filter artifact and may be discarded. The data from the spectroscopy runs on TCU4 bear almost identical results to those discussed for TCU1.

Initially, the magnitude of the features may seem to set the pairs of data runs for TCU2 apart, this may be explained by the sample being removed after the first pair of runs and then reloaded for the second set, meaning that the distance across the gap from the sample to the Kelvin probe varied between the two. Qualitatively, all four sets of data appear very similar: the voltage changes across a band ranging from 1.7 to 2.7 eV with a maximum at 2.1 eV. There is no evidence of contribution from the ZnO band gap, so this is a feature of the BHJ layer. In wavelength terms, sample reacts to light in the 460 to 730 nm range with a maximum at about

6 M. Thirumoorthi, J. Prakash. *Journal of Asian Ceramic Societies* 2016; 4:124–132.
7 H. Kim et. al. J. Appl. Phys. 86, 6451 (1999) and references therein.

590 nm, which closely matches the solar maximum at the surface of the Earth. This means that the solar cell is well-suited to converting solar radiation into electrons with higher conversion efficiencies for the most common solar wavelengths.

While TCU3 also shows evidence of this yellow-centered process, the graph shows that there are likely a number of low-energy processes occurring. There appears to be a low-energy process with a maximum of ~1.6 eV present, as well as a high-energy process that becomes appreciable for photons with energies of 2.8 eV and above.

TCU5's data show the reemergence of the ZnO band gap, which could suggest better electrical contact between the BHJ and ZnO layers, or just indicative of a thinner BHJ layer. The BHJ process centered at 2.1 eV is also evident, but at a much smaller magnitude, which could also be due to a thinner BHJ layer. Unfortunately, there is no available good way to test this individual layer's thickness without some sample destruction due to photodegredation.

Finally, TCU6 shows a mix of the effects evident in the previous samples. Similar to TCU5, both the ZnO band gap and the BHJ process can be seen. The relative magnitudes of the two are reversed, with the a much larger BHJ contribution and a more modest deviation due to the ZnO band gap. A new fluctuation centered around 1.8 eV suggests yet another process. A somewhat similar feature in the graphs of some of the spectroscopy runs on TCU2, the sample with the most similar characteristics to TCU6, hints that this activity could likely be attributed to the presence of the BHJ layer. There is no evidence of such an effect in the data of TCU5, but the predicted magnitude of this secondary BHJ process compared to the main BHJ contribution would be vanishingly small and lost in the noise of the TCU5 graphs. While there initially appears to be yet another process occurring in the 2.5-3.0 eV range, it only shows on two of the spectral runs and is close to a filter change for both, so we can relatively safely discount it.

Surface Photovoltage Studies of Polysulfone Thin Films

Polysulfone Solution Synthesis

To produce our thin films of polysulfone, we used pellets of polysulfone with an average molecular weight of ~35,000 (Sigma Aldrich) as our base material. Using a magnetic stirrer, we dissolved 20 grams of polysulfone in 80 grams of reagent-grade chloroform ($CHCl_3$) from Pharmco-Aaper. The pellets were left in a closed flask to dissolve overnight, which they did. This gave us a 20% polysulfone solution (by weight) from which to produce a dilution series; this solution had an experimental density of 1.32 g/mL.

To create the dilution series, we combined varying amounts of the polysulfone solution with more chloroform to produce 20 mL batches of varying concentrations of polysulfone. Using a micropipette, the correct quantities of the 20% polysulfone solution and chloroform were transferred to clean 20 mL scintillation vials. The quantities are documented in the table below. Due to their lower concentrations of polysulfone, the dilutions did not require more stirring. After adding both fluids to the vial, the solutions could be mixed by hand with a slow swirling motion. The dilutions were then ready for spin coating.

Polysulfone Dilution Series			
% (by mass)	20% PSU (mL)	$CHCl_3$ (mL)	End Volume (mL)
20	20.0000	0.0000	20
15	15.4500	4.5500	20
12	12.5850	7.4145	20
10	10.6173	9.3827	20
9	9.6150	10.3850	20

6	6.5317	13.4680	20
5	5.4777	14.5223	20
3	3.3291	16.6709	20
1	0.8889	19.1111	20

Spin Coating of Polysulfone Thin Films

When spin coating, we used a 6800 Spin Coater Series from Specialty Coating Systems, which required three inputs: compressed nitrogen gas (Matheson Tri-Gas), vacuum (from a Welch Duo-Seal Vacuum Pump), and electricity. The substrate on which the film is deposited is held in place by the vacuum creating a seal against a rubber gasket.

Each spin coating run consists of three steps which in turn possess three variables, RPM (controls spin rate), ramp time (time it takes to reach desired spin rate), and dwell time (amount of time spent at desired spin rate). If a droplet of the polysulfone solution is exposed to air, it quickly forms a skin, which will eventually tear when the droplet is then spun, resulting in an uneven coat. The first step brought the substrate up to a moderate (400-700) RPM and held there for 10 s; this allowed the solution to be applied at speed to promote even coverage. Next, step two brought the sample to a higher spin rate (1350-2200 RPM) to create a relatively uniform surface by removing any excess solution from the sample and allowing the thin film to dry. The final step brings the sample gradually to a stop. The completed samples were marked with their identifying letters and set aside in order; any the promising specimens were placed in plastic sample boxes to minimize the chance of damaging the films.

To create a proper thin film, the substrate needs to be relatively smooth and free from vertical imperfections. Both the microscope slides and the silicon wafers are smooth enough on their own, but they pick up atmospheric particulates while sitting on the shelves. If left on the substrate, these particles would create barriers for the polysulfone mixture, leading to

buildup of polysulfone on the side of the particulate nearest the center of spin and a corresponding dearth of polysulfone in a cone on the opposite side. These "comets" signify an unclean surface that needs to have the physical impurities removed.

When cleaning the microscope slide covers, the samples are placed in a series beakers filled with different chemicals and then run through a cycle in an ultrasonicator to help dislodge the particulates. First, the covers were placed in deionized (DI) water, run through one cycle of the ultrasonicator (about two to three minutes), and then placed in a chloroform bath and ultrasonicated again. The cleaned samples would be left in a chloroform bath until they were set to be used. Due to the need for hand-cutting (which generates dust) as well as their age, the silicon samples required more cleaning than the slide covers. The silicon samples usually cycled through DI water, acetone, methanol, and chloroform baths before being deemed fit to spin-coat. If the spun samples early in the process were showing a significant amount of comets, the latter substrates were run through a longer cycle of DI water, acetone, DI water, methanol, DI water, and chloroform.

Initially, we hoped to test our various spin coating techniques on glass microscope cover slips as they would provide a similar clean surface to the silicon samples, come conveniently sized with no cutting required and no waste generated, and are cheaper than silicon samples. The first 20 samples were spun on the microscope slides with varying degrees of success. A common characteristic emerged on these samples: a concentric ring of polysulfone created a relatively large ridge near the outer edge of the microscope slides. This was theorized to be due to the microscope slides flexing due to the vacuum pressure, forming parabolic dishes instead of flat planes. Due to the increase in height from the center to the edge of the microscope slide, the chloroform was more likely to vaporize near the edges of the slide, leading to a higher deposition rate of polysulfone near the outer edge. When the same

spin coater settings were tested on an n-type silicon sample, which possesses a higher Young's Modulus and is thus stiffer, there was no such uniform ring, so silicon was used for the subsequent samples. Figure 5 shows a cross-sectional representation of the spin coater assembly before the polysulfone is applied.

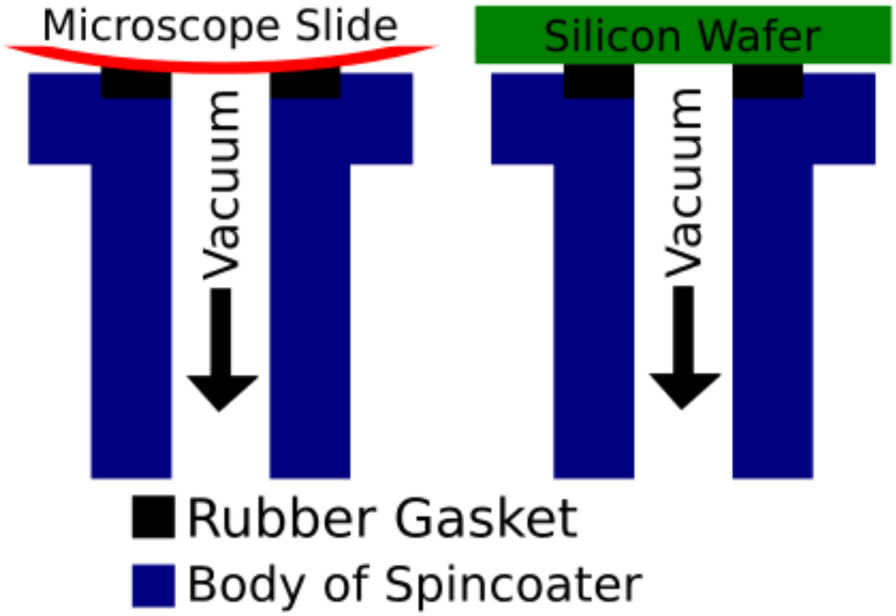

Figure 5: Cross-section of spin coater in operation. Note the flexing in the microscope slide.

During the time that the spin coater took to reach it application speed, it was observed that small air bubbles were infiltrating the micropipette tip. This was due to the high vapor pressure of chloroform at room temperature causing an appreciable amount of the chloroform to boil out of the solution. Therefore, the longer the solution stayed exposed to the air, the more concentrated it became, leaving polysulfone residue behind in the micropipette tips . To combat this, the polysulfone samples which would be used for spin coating were placed in a freezer when not in use, and in an ice bath while spin coating. This lowers the vapor pressure of the chloroform, reducing the rate at which it vaporizes.

One other setback that was encountered took place relatively late in the process. The

1% polysulfone solution became cloudy after some time and, upon testing, would not produce even films. When the vial was inspected, it was discovered that the glue holding the sealing foil in place underneath the cap had been dissolved by the chloroform, contaminating the sample. As there was a very visible change in the vial's contents and a marked decline in the quality of samples that were spun with the contaminated solution, there is little chance that this contamination made it into any of the samples that were tested.

All together, a total of 88 samples were created. As noted earlier, the first 20 samples were spun on microscope slide covers, so they were not going to be tested. Of the remaining 68 samples, most were marred by uneven films caused by defects on the silicon or inconsistent application of the solution while spin coating. Near the boundaries of the wafers, edge effects caused deviations in the film thickness; this is especially noticeable at the corners of the samples. This left us with only a few samples of the requisite quality necessary for surface photovoltage measurements. Ultimately, three samples were chosen for testing: a piece of clean silicon, sample BU (a thin film), and sample AH (a somewhat thicker film than BU).

Experimental

Once we had polysulfone thin film samples that met our criteria, they were tested in a manner similar to the OPV specimens. Each silicon chip to be tested was affixed to the testing stage with a piece of the conductive carbon tape, but we did not need a piece of indium because the silicon is a semiconductor, in contrast to the insulating glass on the solar cells. Each sample was subjected to both transient and spectroscopic testing. After these measurements were taken, sample BU was exposed to UV radiation from a mercury lamp that produces a large amount of 254 nm radiation, transitioning the polysulfone from its natural

hydrophobic state to an alternate hydrophilic state.[8] After irradiation, the polysulfone transitions back to its hydrophobic state over the course of a few hours, so the testing periods for the samples exposed to the ultraviolet light must fit within this time period.[9] Therefore, the sample was allowed a small desaturation period, then exposed to 15 minutes each of white light illumination and darkness for transient testing before being subjected to spectroscopic measurement.

Polysulfone Data and Analysis

Light On SPV Transients

The transient data of the three samples under illumination seem to divide into three overlapping time-scales: short (<30 s), medium (10^1-10^3 s), and long (>10^2 s). In the short term, the silicon control sample possesses a positive logistic growth of ~0.04 V, while the polysulfone of Sample AH appears to reverse the sign on the change, as this sample experiences the almost mirror-image process of a decreasing logistic curve with a magnitude of ~0.04 V. Suggesting that the polysulfone is indeed the culprit of this change is the data from Sample BU, which has a smaller, quick decline in voltage.

All three samples possess almost identical data for the middle region, each having a small ~0.01 V increase with approximately the same start and end points, so this region appears governed by the silicon. Finally, the three plots split apart with different long-term processes. The silicon control sample goes through a logistic process with an increase of 0.06 V. Sample AH appears to have a similar logistic process present, but the polysulfone appears to have increased its magnitude, resulting in a 0.10 V increase. If this were the case, it would

8 C. Sansonetti and J. Reader, *Phys. Scr.* **63**, 219 (2001).
9 Bormashenko.

be expected that the data for BH would lie in between the two graphs; instead, the thinner films unexpectedly produced a smaller increase of only 0.04 V split into two processes that appear to abruptly change at around 10^3 s. However, there is more overall deviation in the illumination data for BU over multiple runs, so nothing definitive might be said about this without further testing of more samples. Each of these long-term processes have inflection points in the 10^3-10^4 range, although the addition of the polysulfone seemed to cause increase the time needed to reach the inflection points of the two polysulfone samples.

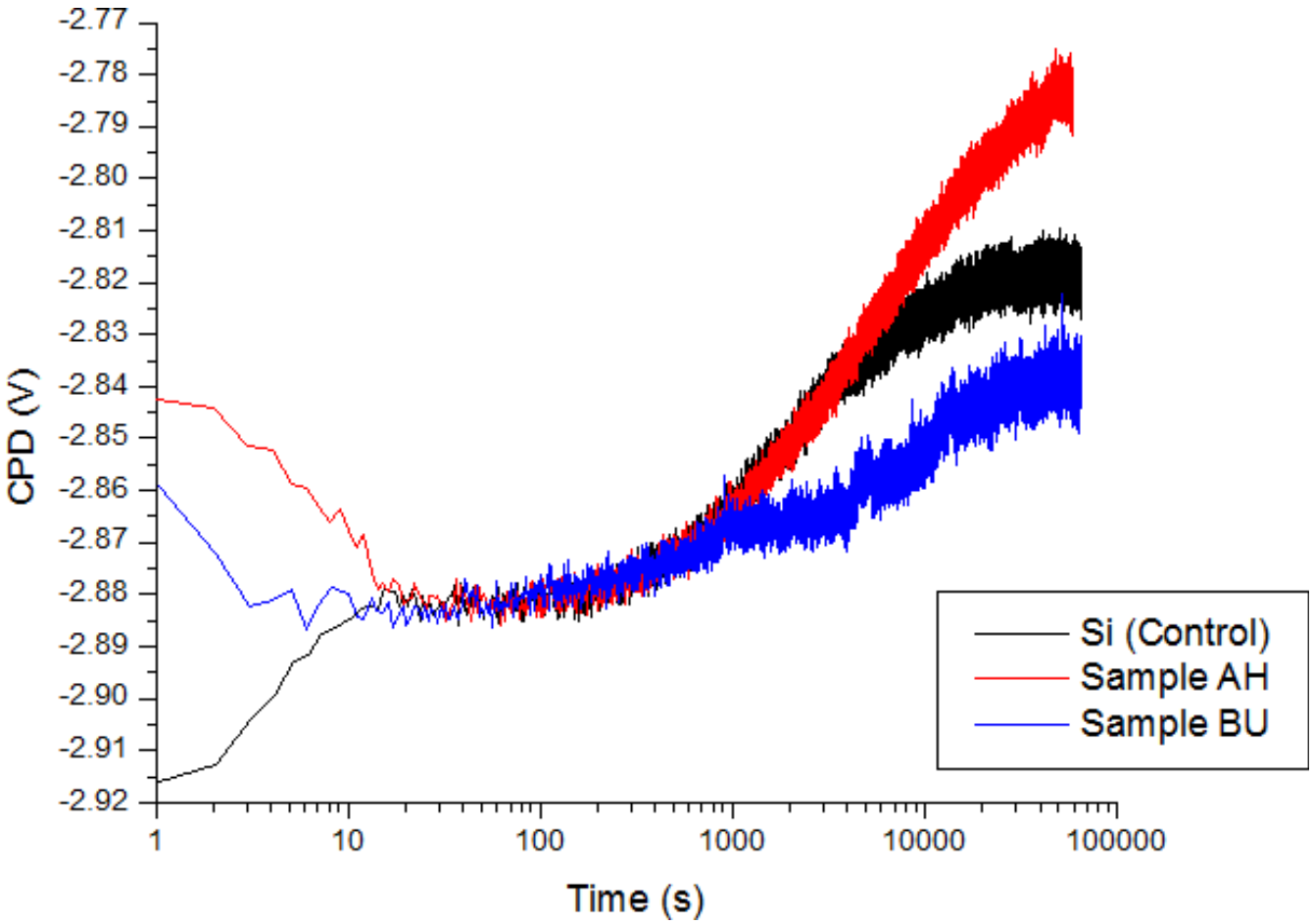

Figure 6: Transient data of polysulfone samples and silicon control when illuminated.

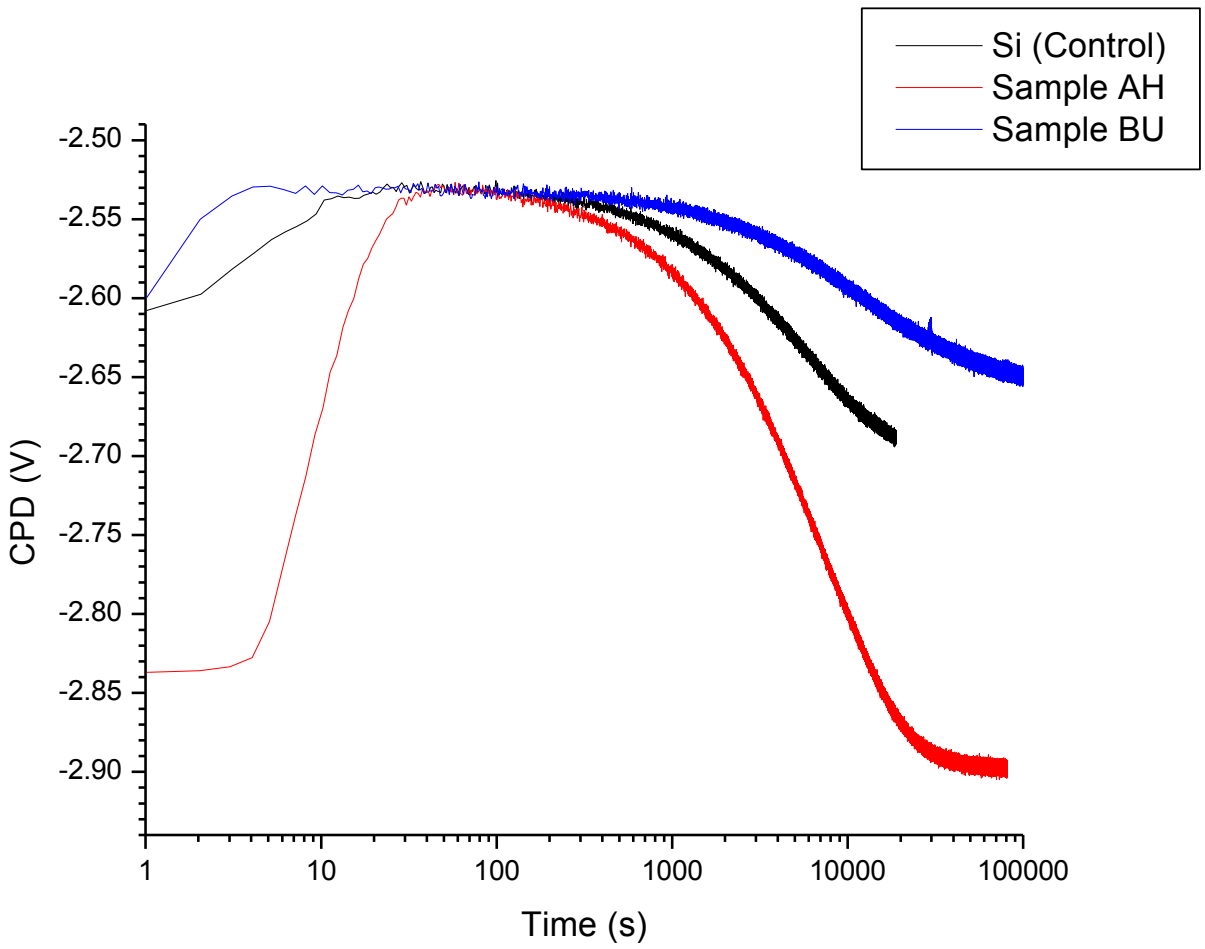

Figure 7: Transient data of polysulfone samples and silicon control in darkness after illumination.

Light Off SPV Transients

Like the data of the samples under illumination, the plots of the samples as the electrons relaxed in darkness share some characteristics and deviate on others. Again, the data may be divided into short (<30 s) and long (>10^2 s) time-scales, with the middle being relatively uniform between the three samples. Both the control and BU had positive logistic curves with magnitudes of ~0.06 V. The quick process in sample AH acts at the same speed, but produces a voltage differential of 0.30 V, five times as large as the other two samples.

All three graphs also had similar negative logistic curve on the long side, as well.

Sample AH produced the largest change of 0.35 V, while sample BU had a more modest change of 0.10 V. The magnitude of the control sample's change again fell in between the other two at ~0.15 V. While AH and the silicon appeared to reach their inflection point in about the same amount of time, BU's inflection point took about almost twice as long to occur.

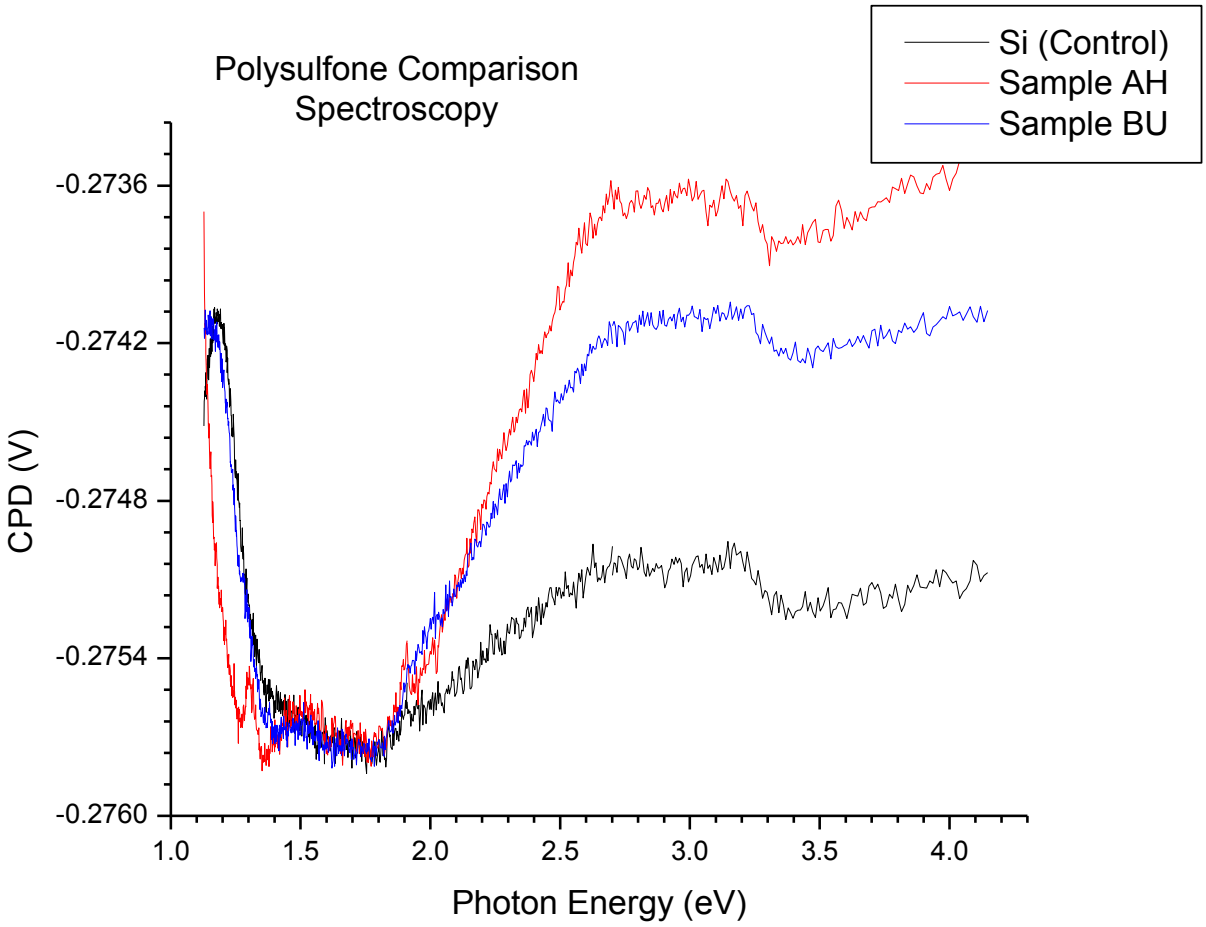

Figure 8: Spectroscopy of polysulfone samples.

SPV Spectroscopy

The relation between voltage and the photon energy also demonstrates the influence of the polysulfone on the measurements. While all three appear to have a maximum at their

leftmost bound, the thickness of polysulfone appears to shift this feature to the decreasing photon energies. When the photons begin to exceed 1.8 eV, the graphs of the three samples begin to diverge, albeit with the same general shape of increasing to a plateau, then a slight dip to a final increase. Each of these features may be seen on all three of the graphs, so they are likely silicon-based processes. The magnitude of these processes appears to be influenced by the polysulfone. The initial increase of BU was twice as large as that of the control, and that of AH was 2.5 times bigger. If this were caused simply by a variation in the separation distance between the Kelvin probe and the sample surface, all the features of each plot would be affected, not just this particular region.

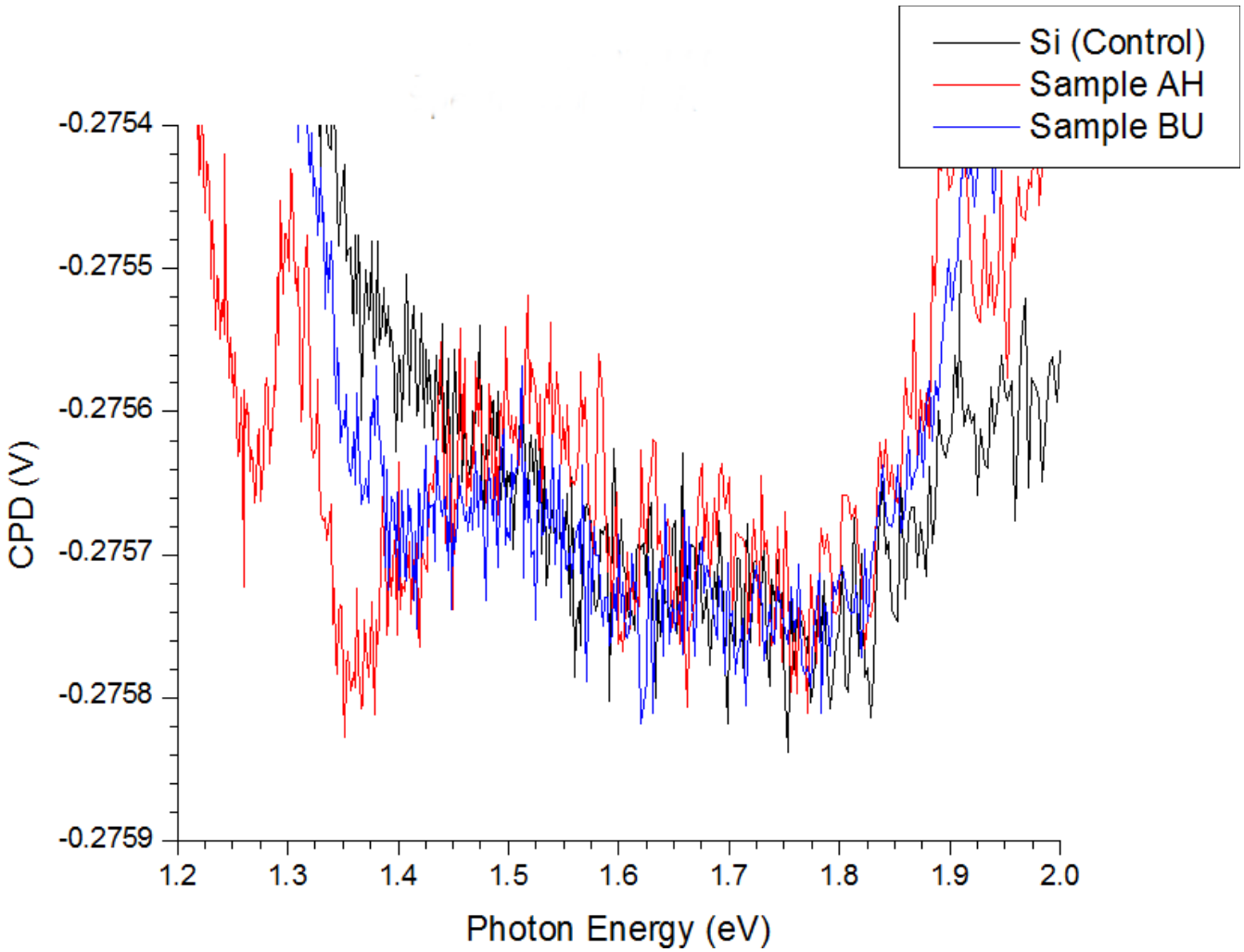

Figure 9: Enlarged view of near-infrared region of the previous polysulfone spectroscopy plot.

A close-up of the near-infrared region of the spectral graphs reveals more individual features that can likely be attributed to the polysulfone films. Two minima and a maximum appear in the AH and BU sample graphs in the 1.25-1.45 eV range that are not present in the silicon control sample. After 1.45 eV, the sample graphs converge and continue onwards. While this data might be used to construct a band diagram normally, the deviations in the gap state's energies due to sample thickness require more data before a quantitative graph might be drawn.

Effects of UV Processing

Moving onwards, the graph of the UV-exposed polysulfone sample under illumination did provide some interesting data. As there were no previous surface photovoltage studies performed on UV-altered polysulfone that we are aware of, this was more of a fact-finding mission than true analysis.

Under illumination, the UV-irradiated sample exhibits an initial fast process (<10s) resulting in a decrease of 0.090 V, while the unaltered sample shows the same initial change, but at a much more modest 0.025 V. After this point, in time, the voltage for the unaltered sample increased slowly, but the altered sample shows more activity. In the 10-300 s range, the sample experiences both a rise and fall in voltage, possibly from some of the electrons that were initially trapped finding channels to redistribute along. The data then shows a general upward trend in voltage with some fairly regular deviations. Knowing that the polysulfone recovers to its original state over time, the variations in the tail data could be attributed to these changes in structure. Due to this time constraint, the slow and very slow processes could not be measured.

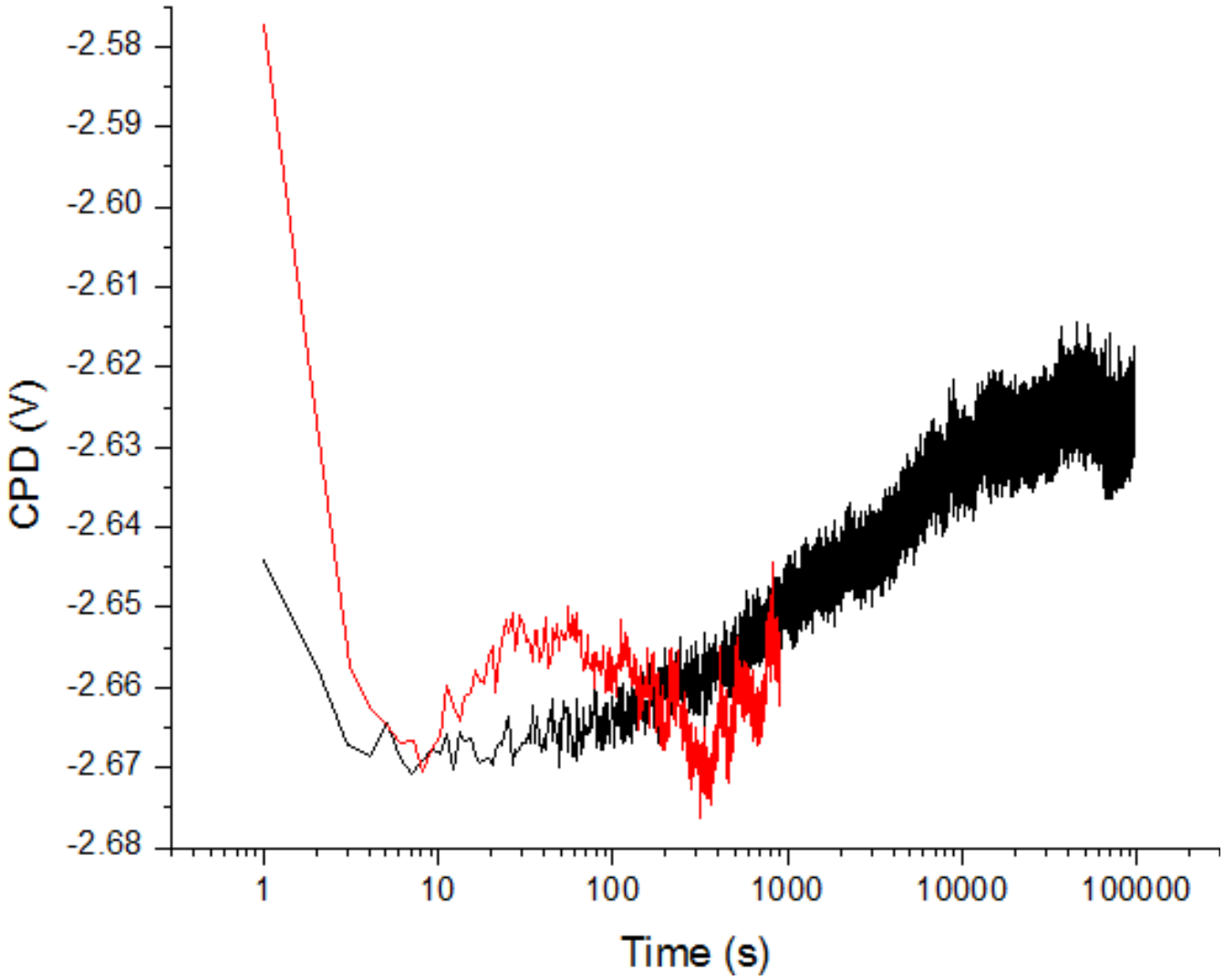

Figure 10: Transient data of polysulfone thin film BU under illumination. Untreated run in black; UV-exposed in red.

When compared to the normal state, being exposed to UV light only produced minor changes on the desaturation curves. The only change of any significance apparent is a light increase in the initial voltage jump 0.10 V versus 0.06 volts for the sample in its natural state. As in the illumination graph, there are regular deviations in the tail of the altered sample's data. These features being present in both the illuminated and darkened environment suggest that they could indeed be due to the polysulfone's reversion process. The tail of the graph also

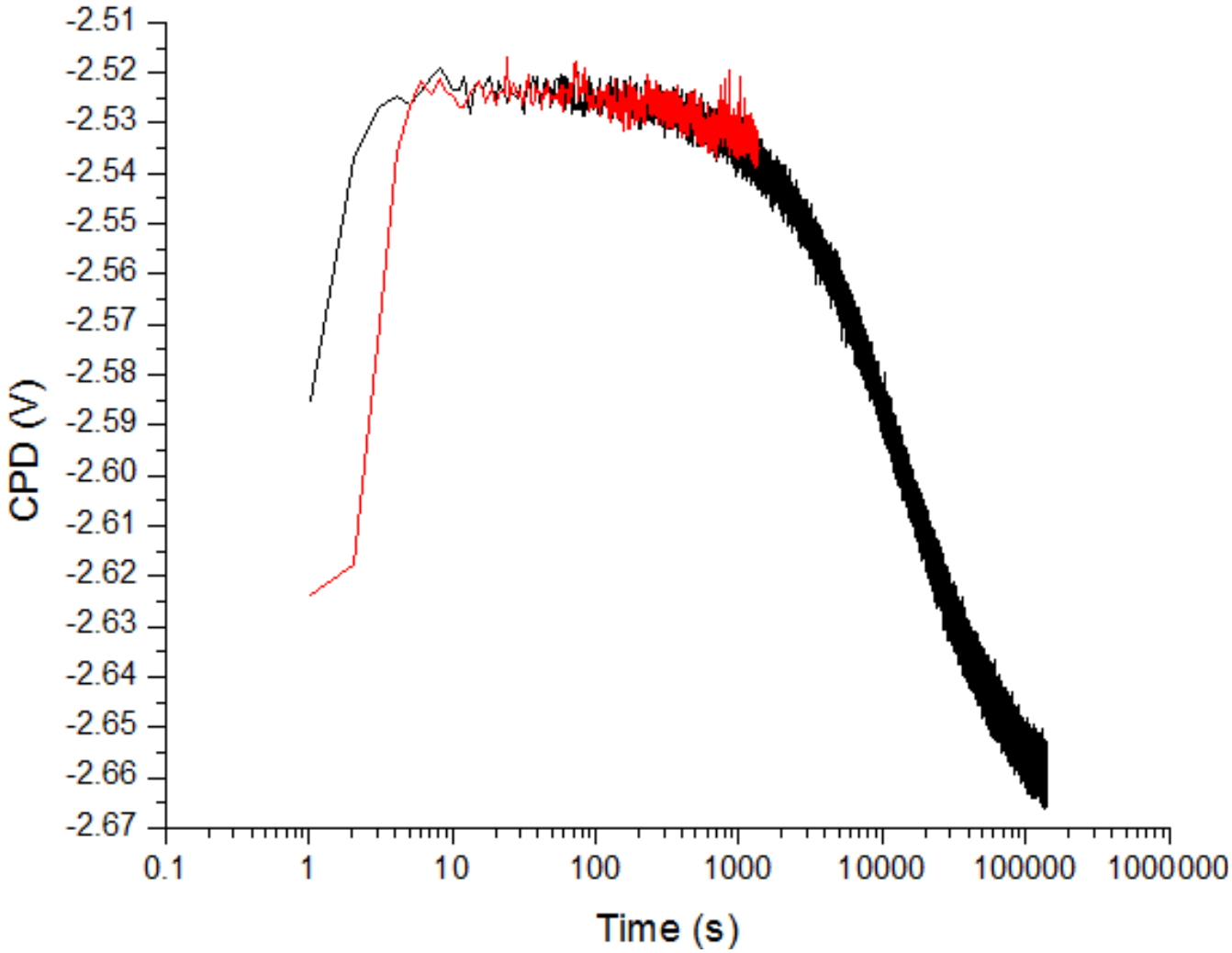

Figure 11: Transient data of polysulfone thin film BU in darkness after a period of extended illumination. Untreated run in black; UV-exposed in red.

begins to deviate from the control data, but due to the relatively short time-frame in which these samples could be tested, it was not possible to observe whether the exposure to UV light created or changed any of the slow processes already present.

Although the signal-to-noise ratio of the altered sample's data may be higher, the spectroscopy still shows some significant difference between the two. A peak in the UV-irradiated sample's data appears in the near-infrared at 1.5 eV which is not seen in unaltered sample's measurements. Another new (and much wider) peak is also visible in the 2.7-3.4 eV

range.

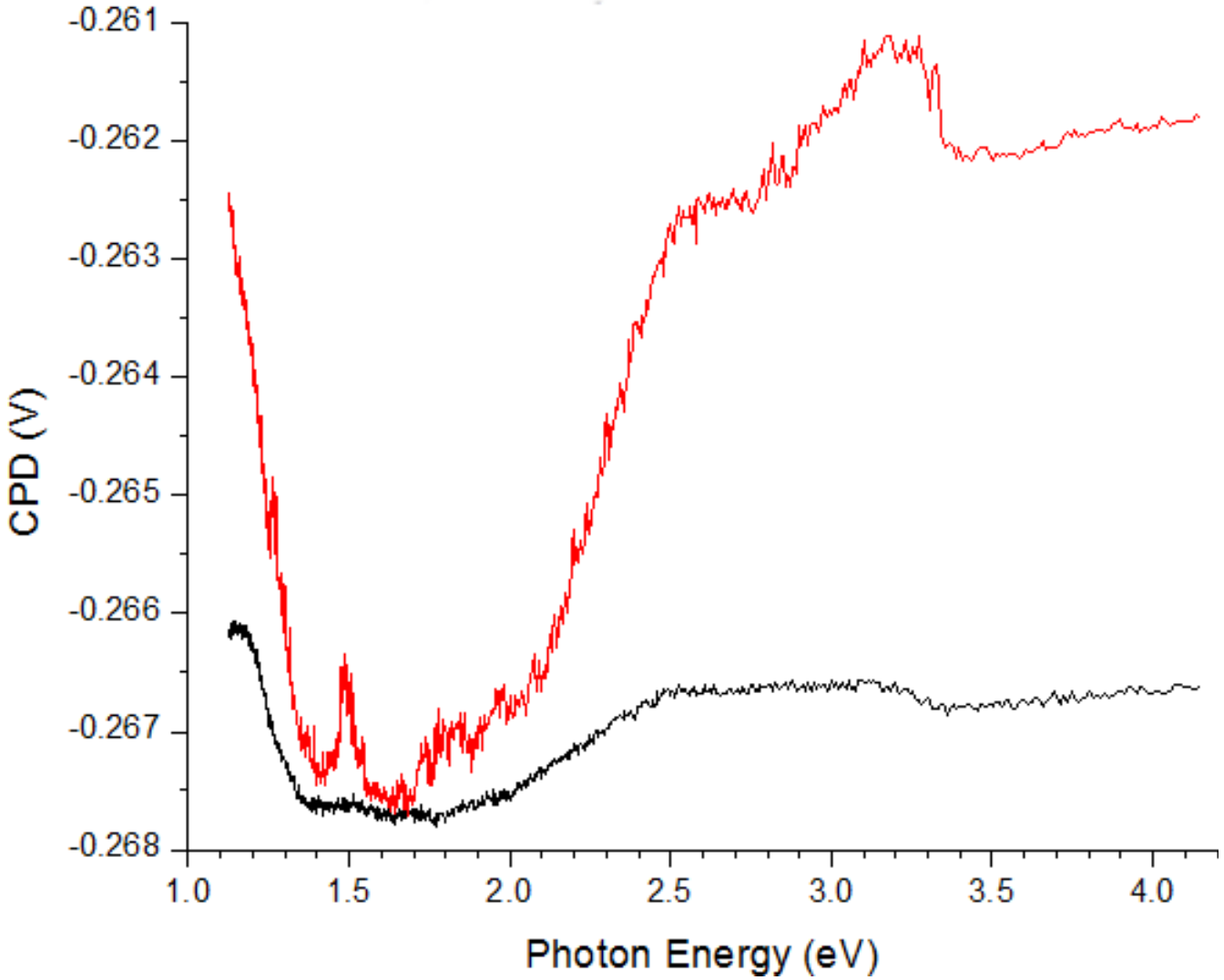

Figure 12: Comparison of spectral measurements for hydrophobic and hydrophilic surfaces. Untreated run in black; UV-exposed in red.

Conclusion

These two projects highlight two distinct applications of surface photovoltage as applied to polymer films. As in crystalline semiconductor samples, both the effects of the uppermost surface as well as those of the buried interfaces were evident. The results shed light on both the overall structure of the materials' band diagrams and the changes they undergo due to the addition or modification of a layer.

For the BHJ solar cells, the results suggested optimum annealing temperatures for the samples and provided some hint as to the photon energies that best produce electrons. Under illumination, the polymer layer added a positive rebound effect in the intermediate timescale between negative trends in the small and large timescales. For the measurements taken in darkness, the polymer layer exhibited a quick positive increase followed by a slow decline, in contrast to that of the samples without a polymer layer which only demonstrate a medium-to-long timescale positive increase. The addition of the polymers also decreased the magnitude of the observed effects attributed to the Glass, ITO, and ZnO layers. The spectral data shows the existence of an absorption peak near the solar maximum, an encouraging sign for future development.

When working with the polysulfone, a successful method was developed to produce films of variable thickness on silicon substrates, and these films were again tested with surface photovoltage techniques, yielding information that some evident states vary with the thickness of the film. Not only did the deposition of polysulfone amplify the overall surface photovoltage signal, it also added more characteristics to the transient and spectral data, most notably reversing the polarity of the fast transient features in the darkened measurements. The polysulfone also added more peaks in the near-infrared area of the spectral data as well as red-shifting the apparent band-gap transition of the silicon substrate. A polysulfone film

was also exposed to UV radiation, and the surface photovoltage data of this altered state was compared to the initial data, yielding a number of features in both the transient and spectral data that may be attributed to the change in state.

From these two experiments, we have confirmed that surface photovoltage can be used to investigate the optoelectronic properties of thin polymer films. Each test subject yielded more information on the topic of study, as well as honing a number of skills essential to the nascent researcher. This year-long process has been a wonderful learning opportunity, providing numerous ways to learn both the specific craft as well as general abilities that can be applied broadly in many disciplines.

Appendix A: Solar Cell Spectroscopy Plots

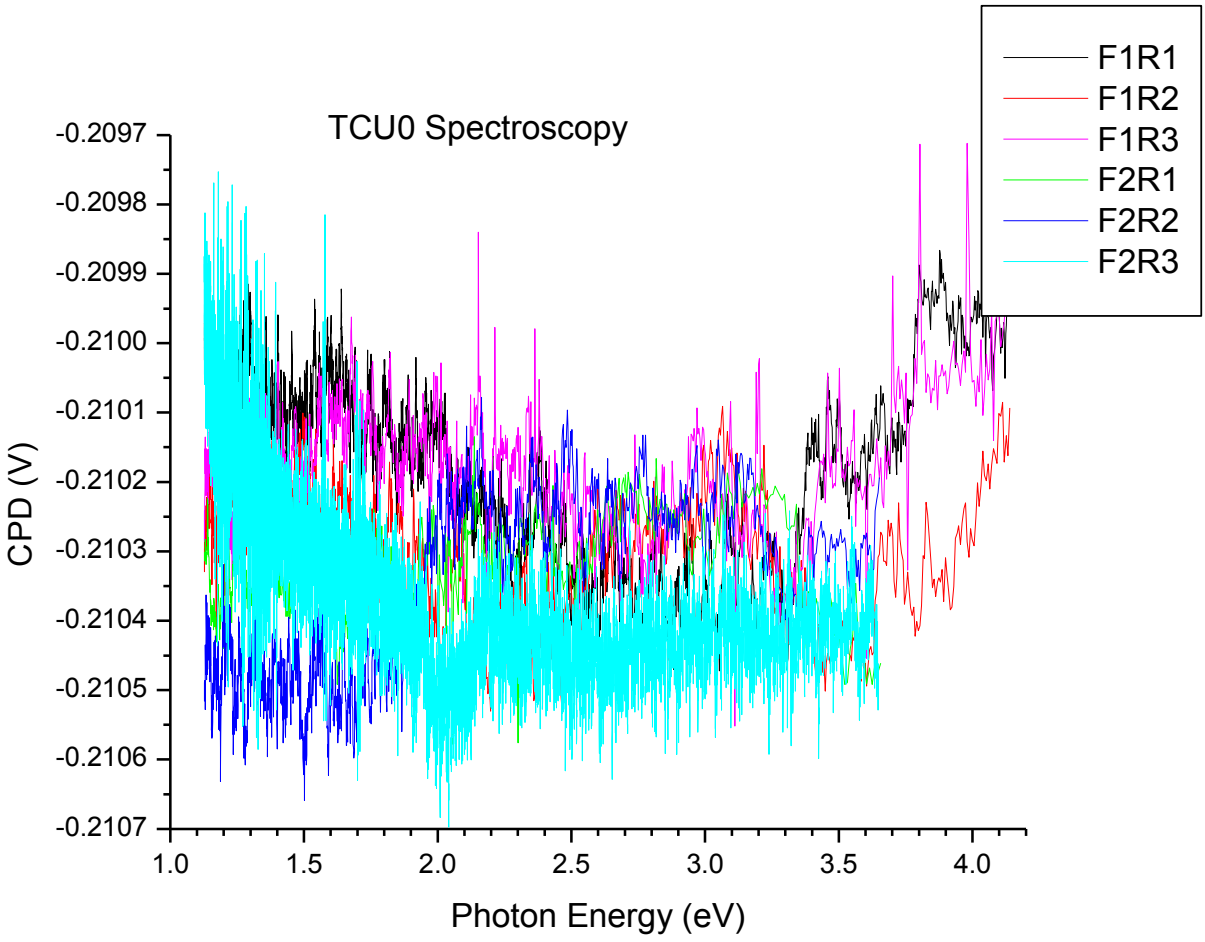

Figure 13: Surface photovoltage spectroscopy data from TCU0.

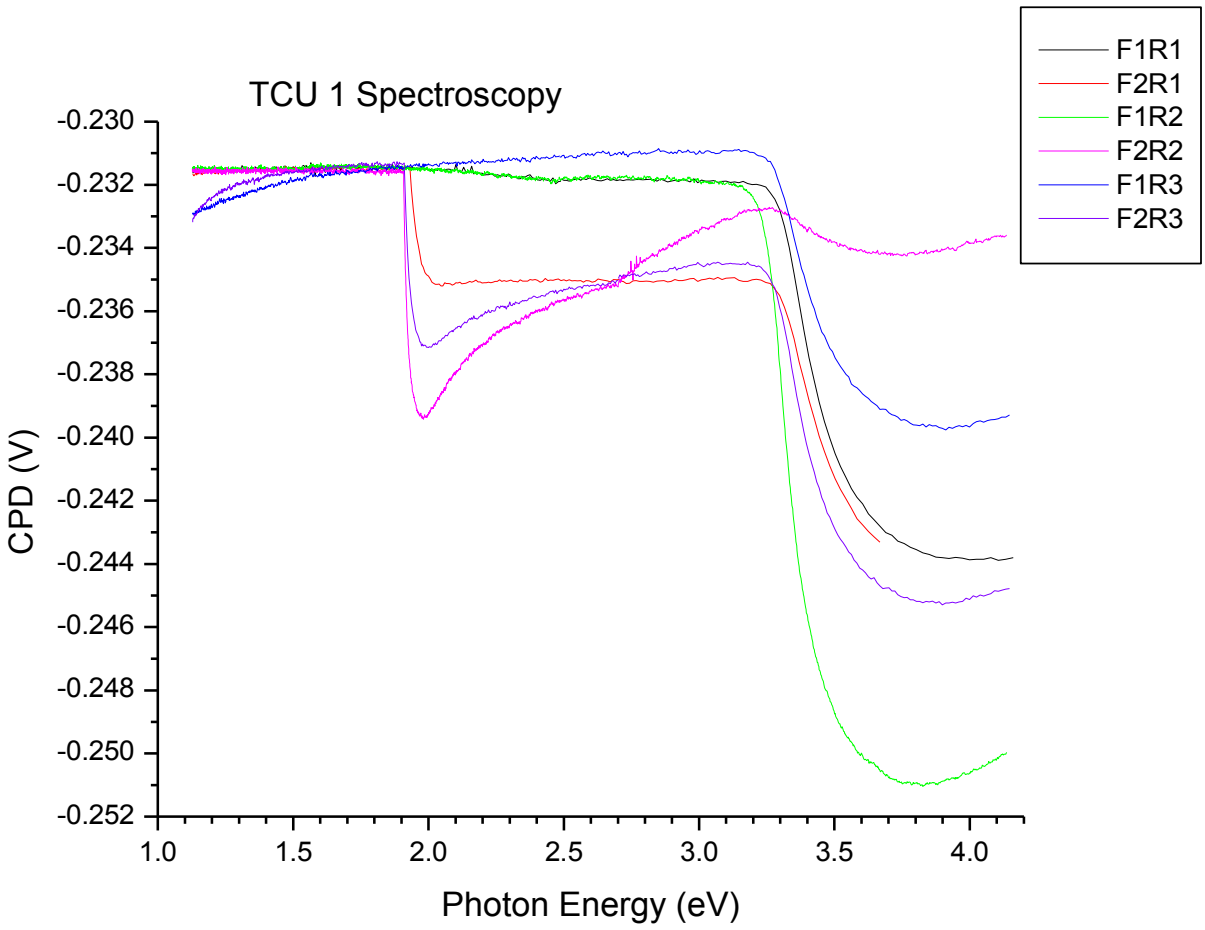

Figure 14: Surface photovoltage spectroscopy data from TCU1.

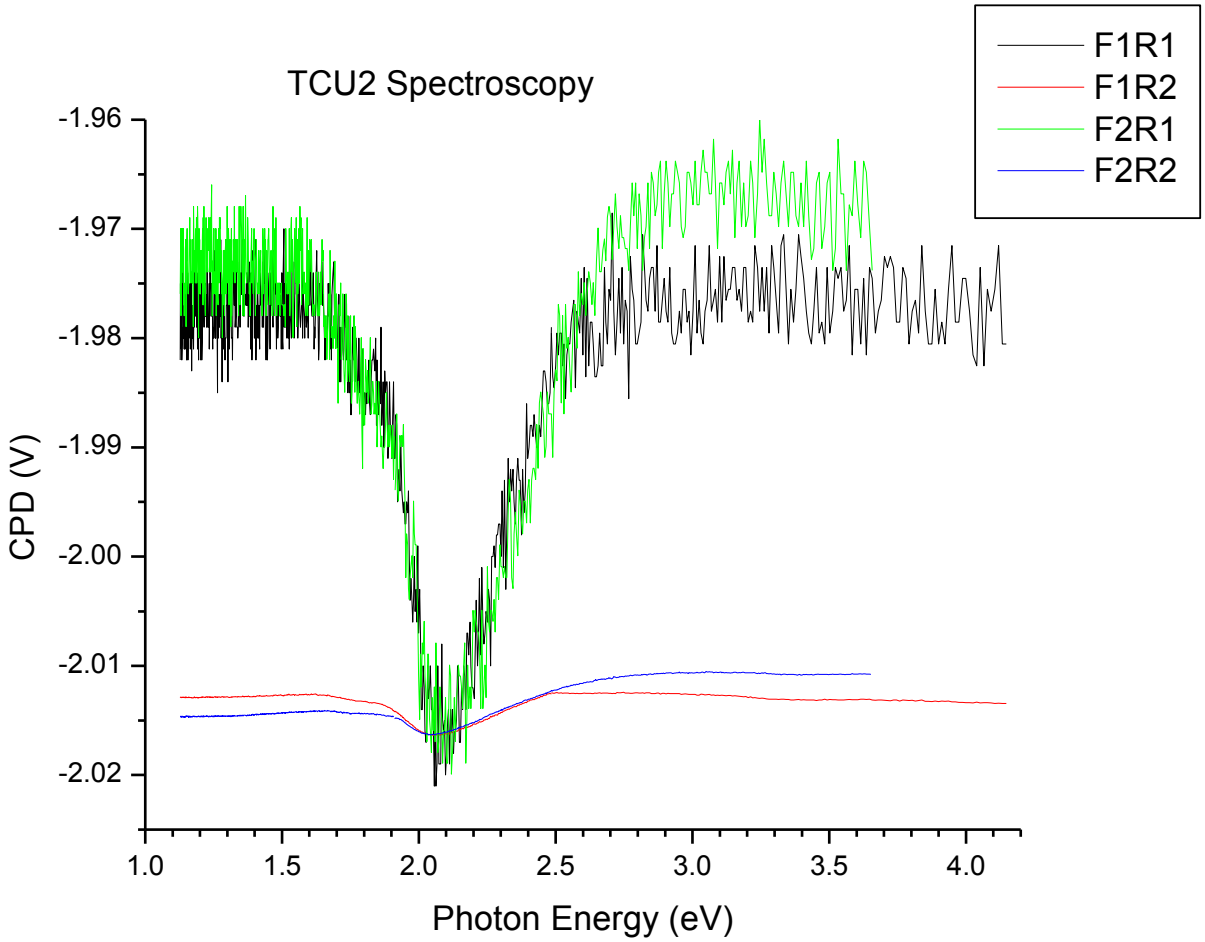

Figure 15: Surface photovoltage spectroscopy data from TCU2.

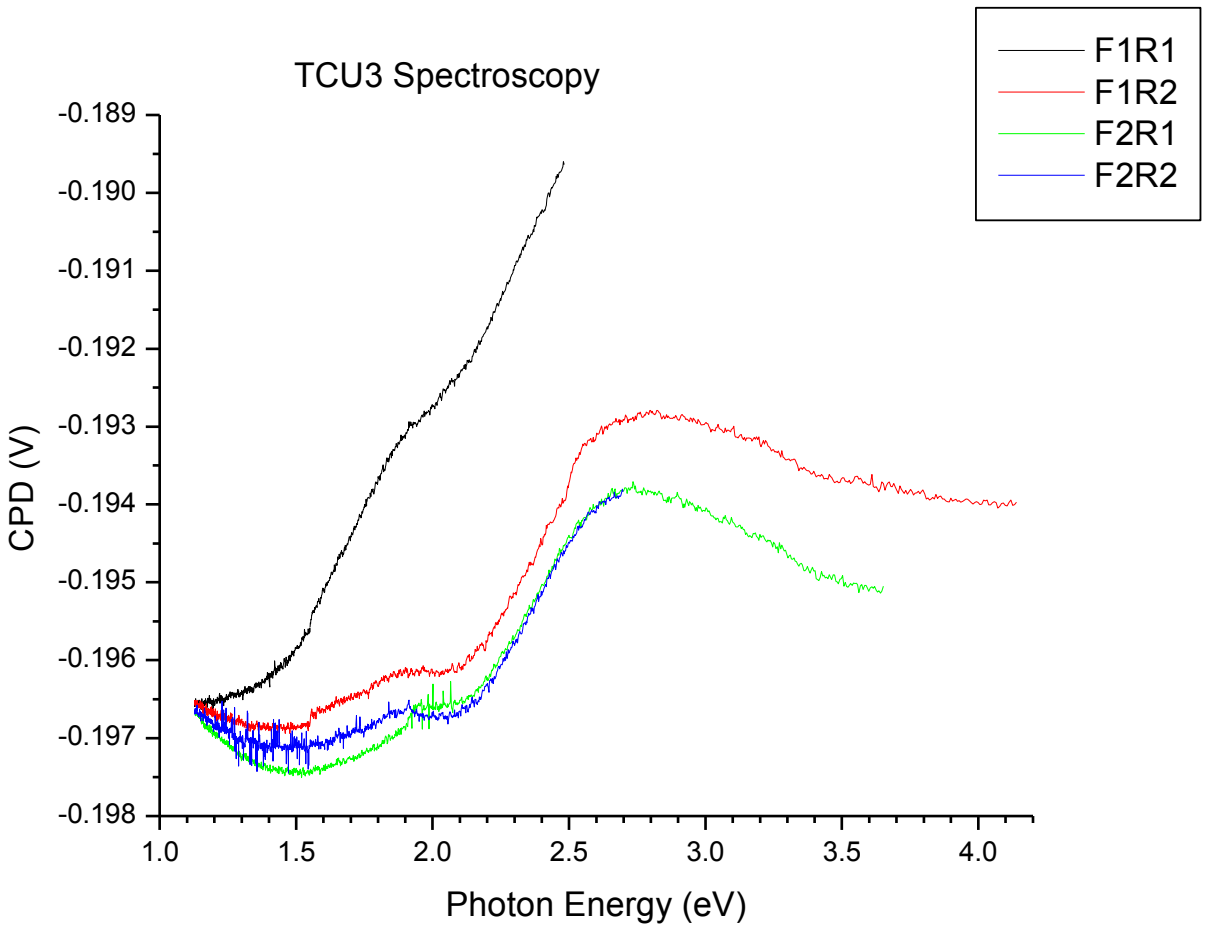

Figure 16: Surface photovoltage spectroscopy data from TCU3.

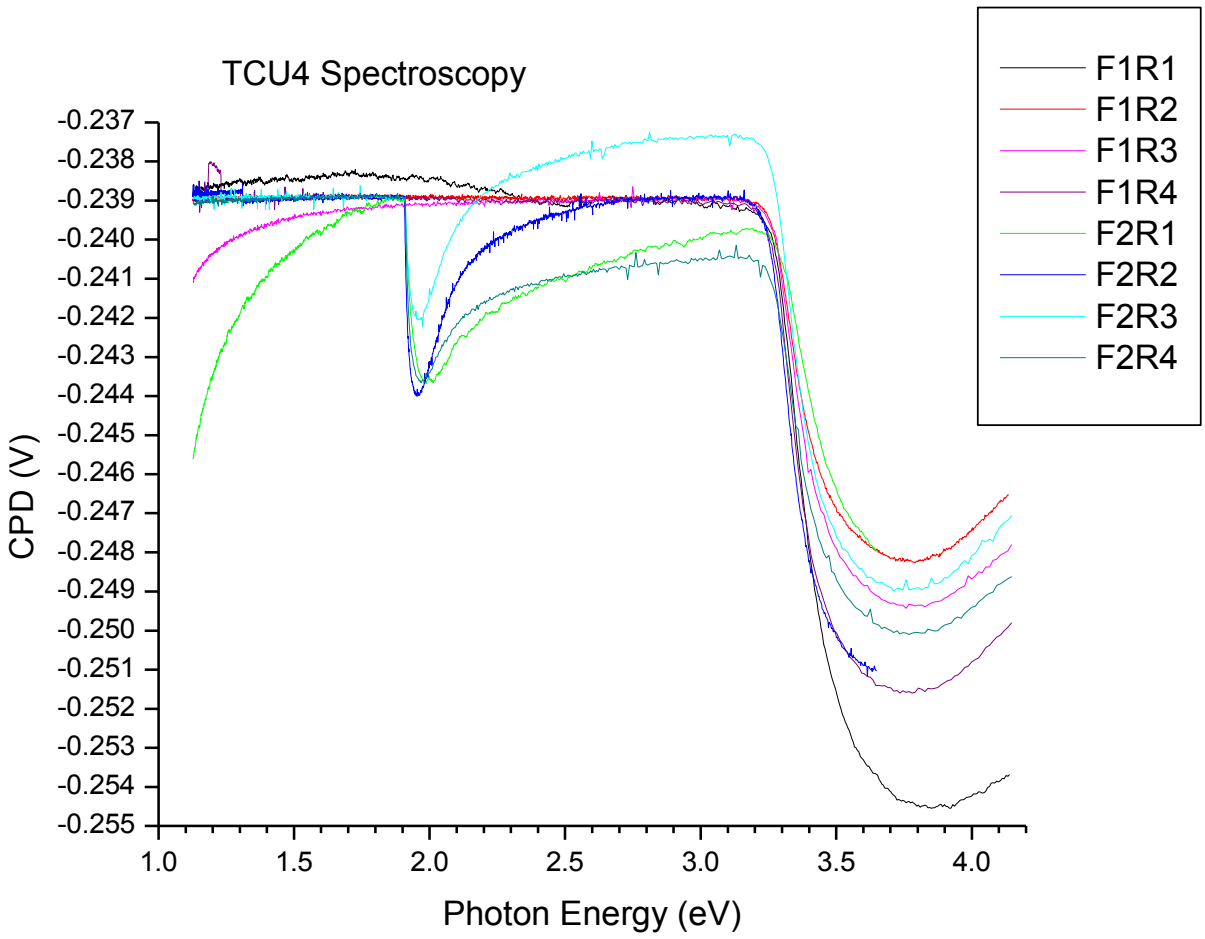

Figure 17: Surface photovoltage spectroscopy data from TCU4.

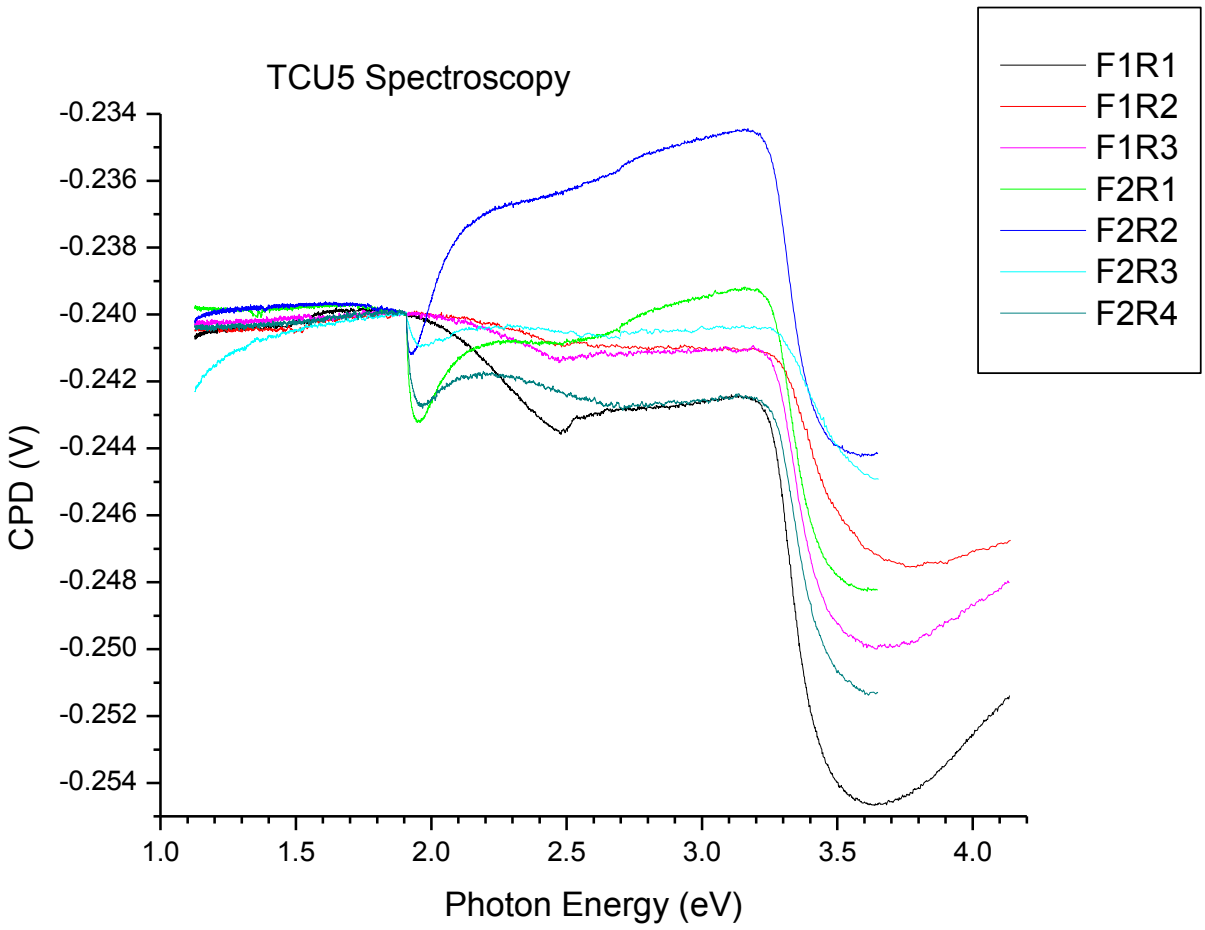

Figure 18: Surface photovoltage spectroscopy data from TCU5.

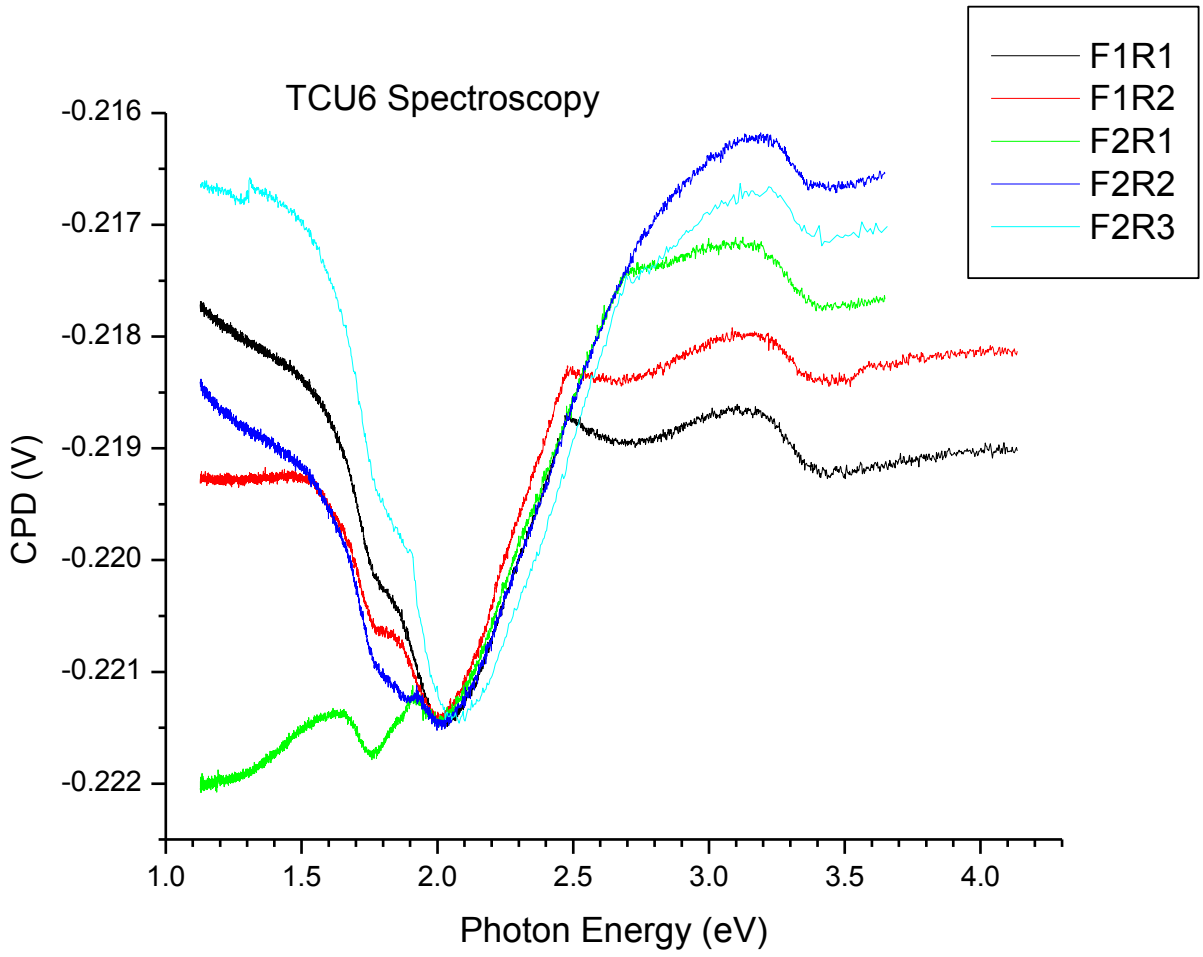

Figure 19: Surface photovoltage spectroscopy data from TCU6.